RSC Advances

PAPER

View Article Online
View Journal | View Issue

Cite this: *RSC Adv.*, 2015, **5**, 48164

Carbon nanotube-based super nanotubes: tunable thermal conductivity in three dimensions†

Haifei Zhan, John M. Bell and Yuantong Gu*

Received 30th March 2015
Accepted 19th May 2015

DOI: 10.1039/c5ra05584a

www.rsc.org/advances

Advances in nanomaterials/nanostructures offer the possibility of fabricating multifunctional materials for use in engineering applications. Carbon nanotube (CNT)-based nanostructures are a representative building block for these multifunctional materials. Based on a series of *in silico* studies, we investigated the possibility of tuning the thermal conductivity of a three-dimensional CNT-based nanostructure: a single-walled CNT-based super-nanotube. The thermal conductivity of the super-nanotubes was shown to vary with different connecting carbon rings and super-nanotubes with longer constituent single-walled CNTs and larger diameters had a smaller thermal conductivity. The inverse of the thermal conductivity of the super-nanotubes showed a good linear relationship with the inverse of the length. The thermal conductivity was approximately proportional to the inverse of the temperature, but was insensitive to the axial strain as a result of the Poisson ratio. These results provide a fundamental understanding of the thermal conductivity of the super-nanotubes and will guide their future design/fabrication and engineering applications.

1. Introduction

Recent advances in nanotechnology have contributed to the continuing miniaturization of devices and offer the possibility of fabricating multifunctional materials for use in a wide range of engineering applications, including adaptive airfoils and robotic skins.[1] Nanoelectromechanical systems that respond to an extremely small change in mass or force as a result of their integrated sensors and electronic circuits[2] are at an early stage of development. As the building blocks for these multifunctional materials, low-dimensional carbon materials, such as carbon nanotubes (CNTs) and graphene, have received much interest from both the scientific and engineering communities. Atomically thin graphene shows great promise in applications such as portable and wearable energy conversion and storage devices (*e.g.* fuel cells and supercapacitors).[3] The versatility of carbon in forming different hybridization states allows the fabrication of various carbonaceous nanomaterials/nanostructures from zero- to three-dimensional (3D), realizing different desired functionalities.[4] For example, the thermal transport properties of two-dimensional (2D) carbon networks can be effectively altered by changing the structure.[5] A recently synthesized 3D CNT pillared graphene structure[6] shows wide-ranging prospects for applications as thermal sinks in electronic devices.[7]

Among the various carbon-based nanostructures, CNT-based nanostructures, such as 3D CNT–graphene hybrid nanostructures,[8] 2D super-graphene[9] and 3D super-carbon nanotubes (STs),[10] have received the most interest. STs are constructed by replacing the C–C bond with a single-walled CNT (SWNT). It has been reported that these STs show both metallic and semiconducting behavior,[11] high flexibility[12] and ultra-high sensitivity as a mass sensor (about 10^{-24} g).[13] The majority of studies have focused on the mechanical properties of STs, *e.g.* the mechanical behavior under tension,[14] compression and bending.[15] However, to facilitate the various promising applications of STs, such as fuel cells, battery electrodes or nanoelectronic devices, a comprehensive understanding of their thermal transport properties is needed.

Previous studies have shown that the strength, stiffness and toughness of ST can be optimized simultaneously during construction.[16] In this work, we used large-scale molecular dynamics (MD) simulations to assess the thermal conductivities of STs with various geometrical structures and sizes at different temperatures and strain status. These results establish a basic understanding of the thermal conductivities of STs and will guide their future design and applications.

2. Computational methods

The thermal conductivity (κ) of the STs was calculated based on the Muller–Plathe method,[17] known as reverse non-equilibrium MD simulations. Before the calculation, the configuration of the

School of Chemistry, Physics and Mechanical Engineering, Queensland University of Technology, GPO Box 2434, 2 George St, Brisbane, QLD 4001, Australia. E-mail: yuantong.gu@qut.edu.au; Fax: +61-7-31381469; Tel: +61-7-31381009

† Electronic supplementary information (ESI) available: The atomic configurations of ST's unit cells made from (6,6) SWNTs, and the stress–strain curves of the ST under axial strain. See DOI: 10.1039/c5ra05584a

STs was first optimized using the conjugate gradient minimization method and then equilibrated using the Nose–Hoover thermostat[18,19] under ambient conditions for 500 ps (temperature 300 K, pressure 1 atm). A constant heat flux (J) was then introduced to the system through a velocity exchange scheme under the microcanonical ensemble, *i.e.* the NVE ensemble with constant atom number, volume and energy. κ was then calculated when the system arrived at the steady-state regime according to $\kappa = -J/(\partial T/\partial x)$. Here, $\partial T/\partial x$ is the temperature gradient along the heat flux direction (x) and J is the heat flux computed from

$$J = \frac{1}{2tA}\sum_{N}\frac{m}{2}\left(v_{\text{hot}}{}^2 - v_{\text{cold}}{}^2\right) \quad (1)$$

where t is the total simulation time, N is the total number of exchanges, m is the atomic mass, v_{hot} and v_{cold} are the exchange velocities of the hot and cold atoms, respectively, and A is the cross-sectional area. The factor 2 in the denominator is used to account for the periodicity of the system. To ensure a reliable thermal conductivity, κ was calculated at a time interval of 250 ps for a total simulation time of 4 ns and averaged over the simulation duration from 3 to 4 ns. During the whole simulation, a small time step of 0.5 fs was chosen and the C–C atomic interactions were modeled by the widely used adaptive intermolecular reactive empirical bond order potential method,[20] which has been shown to be a good representation of the binding energy and elastic properties of carbon materials. Periodic boundary conditions were applied along the length direction of the STs. The whole calculation was performed using the software package LAMMPS.[21]

3. Results and discussion

3.1 Influence of structure

We initially determined the thermal conductivity of the STs with different structures. Fig. 1 shows that different architectures can be obtained by altering the dimensions of the constituent SWNTs (both radius and length), the chirality of the STs and also the atomic configurations at the junctions. Fig. 1b shows the top view of three different junction types (denoted as α, β and γ), in which three constituent zigzag (8,0) CNTs are connected by six heptagons, six adjacent heptagons and six pairs of pentagons and octagons, respectively. The STs constructed from (n, m) SWNTs are denoted as ST(N, M)@(n, m)-α (α representing the junction type). Thus the radius of the ST can be calculated from

$$R_{\text{ST}} = l_{\text{cnt}}\sqrt{3(N^2 + MN + M^2)}\Big/(2\pi)$$

where l_{cnt} is the distance between the adjacent junctions (Fig. 1a)[14] – that is, the outer and inner radii of the STs are equal to

$$R_{\text{ST}} + d_{\text{cnt}}/2 \text{ and } R_{\text{ST}} - d_{\text{cnt}}/2$$

where d_{cnt} is the diameter of the constituent SWNTs, respectively. The three ST models discussed initially consist of (8,0) SWNTs, which share a similar size with the same l_{cnt} of about 19 Å. As a result of the highly porous nature of the STs, we approximate the cross-section as a continuous annulus – that is, the cross-sectional area is approximated as $2\pi R_{\text{ST}}d_{\text{cnt}}$ when calculating the heat flux from eqn (1) (refer to Section 2). Note that such an approximation should not influence the discussion as we will focus here on the relative thermal conductivity of the various STs.

In general, a relatively low thermal conductivity was estimated for the different STs. κ for the ST(5,0)@(8,0)-α is about 5.4 $\pm$ 0.1 W mK^{-1}. Such a low thermal conductivity was a result of the continuum approximation of the highly porous structure of the STs, which will greatly increase the cross-sectional area (Fig. 1a). With reference to eqn (1) (refer to Section 2), the much larger cross-sectional area of the STs compared with that of the SWNTs will greatly reduce the calculated thermal conductivity (see ESI† for a more detailed discussion). The left-hand panel of Fig. 2a shows that the junction type plays an important role in the thermal transport properties of the STs. For all three junction types [ST(5,0)@(8,0), STs with a diameter of about 6 nm and a length of about 75 nm], the effective κ of the ST with β junctions is about 36% larger than its counterpart with α junctions. The origins of such a difference can be evidenced by looking at their vibrational density of states (VDOS, computed from the Fourier transformation of the autocorrelation function of the atomic velocities[22]). As seen in Fig. 2b, the VDOS spectrum varies with the junction type, which therefore endows the ST with various thermal conductivities. In general, the ST exhibits a similar but shifted pattern of VDOS compared with the SWNTs with low-frequency (out-of-plane) and high-frequency (in-plane) phonon modes around 20 and 60 THz, respectively. However, unlike SWNTs, where the amplitude of the high-frequency component is much larger than that of the low-frequency component, the ST shows a similar amplitude for both the low- and high-frequency components. Such an observation indicates that the out-of-plane phonons also play an important role in the thermal transport properties of the ST as a result of its 3D structure.

We then looked at the thermal conductivity of the STs with a similar geometric size, but different constituent CNTs [ST(6,0)@(6,6), see the ESI† for atomic configurations]. The ST(6,0)@(6,6) has an l_{cnt} of about 15 Å, with an outer radius of about 29 Å, similar to the radius of the ST(5,0)@(8,0). As illustrated in the center panel of

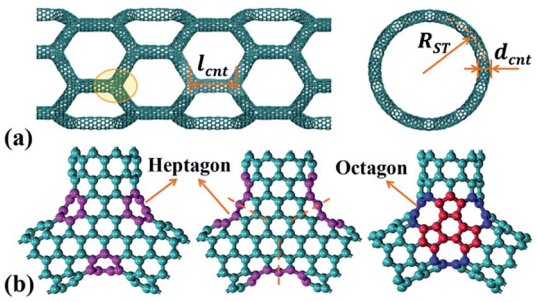

Fig. 1 (a) Atomic configuration of a ST. (b) Three different junctions constructed by (8,0) SWNTs, denoted from left to right as (8,0)-α, (8,0)-β and (8,0)-γ. The connecting pentagons, heptagons and octagons are highlighted in red, magenta and blue, respectively.

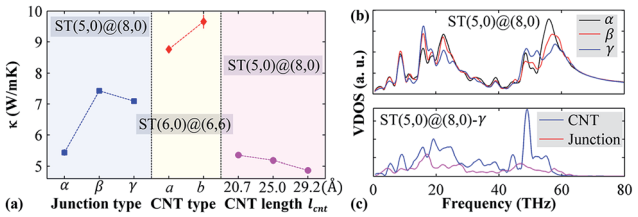

Fig. 2 (a) Thermal conductivity of different STs; the error bar represents the standard deviation of the thermal conductivity for a simulation time of 3–4 ns. (b) Comparisons of the VDOS between different junction types. (c) Comparisons of the VDOS at the CNT and junction regions.

Fig. 2a, the effective κ of the two STs constructed from armchair (6,6) SWNTs is much larger than that of the ST made from (8,0) SWNTs. For instance, the effective κ of the ST(6,0)@(6,6)-β is more than 80% larger than the κ of the ST(5,0)@(8,0)-α. This observation suggests that the thermal conductivity of the ST can be tuned by altering the chirality of the constituent CNTs. There are two possible origins responsible for the large difference in the thermal conductivity between the ST(5,0)@(8,8) and ST(6,0)@(6,6). First, different constituent CNTs require different connecting carbon rings, which will induce different VDOS from those in Fig. 2b and therefore result in different thermal transport properties. Fig. 2c shows that there are evident mismatches in the VDOS between the CNT and junction regions and such VDOS mismatches are determined by the connecting carbon rings at the junctions. Second, different constituent CNTs mean different geometric sizes of the STs, including the cross-sectional thickness and radius. This geometrical difference exerts a significant impact on the thermal transport properties of the ST. The right-hand panel of Fig. 2a compares the effective κ values for STs with the same constituent CNTs and similar lengths of STs, but different lengths of the CNTs (l_{cnt}). Although the STs with longer constituent CNTs had fewer junctions (less phonon scatterings), a lower thermal conductivity was observed. This phenomenon can be explained by considering the impact of the diameter of the STs as discussed in the following section by noting that the diameter of the STs increases with increasing length of the constituent CNTs.

3.2 Size and temperature dependence

In addition to the evident geometrical impacts on the thermal conductivity of the ST, κ is also sensitive to the sample size (length and radius). According to the common heuristic argument that when the periodic length of the simulation cell L_{cnt} is smaller than the phonon mean-free path Λ (Λ is about 700–750 nm for SWNTs at room temperature[23]), the inverse of the thermal conductivity is proportional to the frequency of the scattering events, with contributions from the sample ends and from intrinsic scattering:[24,25]

$$1/\kappa \propto 1/\Lambda + 1/L_{cnt}$$

Consistent with such an assumption, the inverse of κ showed a good linear relationship with the inverse of the length of the STs (Fig. 3a). By extrapolating the linear trend to $L \sim \infty$, the limit of thermal conductivity for a macroscopic ST κ_∞ can be obtained. Fig. 3a shows that the limit of thermal conductivity for the ST(5,0)@(8,0)-γ was estimated as $\kappa_\infty = 5.9\ \mathrm{W\ mK^{-1}}$ – that is, κ will saturate to κ_∞ at 300 K when the sample size is much larger than the phonon mean-free path.

The dependence of the effective κ on the diameter of the STs was also examined. Fig. 3b shows that the effective κ decreases gradually and continuously with increasing diameter of the STs, which agrees with the results reported for SWNTs.[26] Theoretically, the heat in the ST is mainly transferred by lattice vibrations resulting from the strong covalent sp^2 bonds. The lattice thermal conductivity at a given temperature is expressed as:[27]

$$\kappa(T) = \sum_j C_j(T) v_j^2 \tau_j(T) \quad (2)$$

where C_j, v_j and τ_j are the specific heat, phonon group velocity and phonon relaxation time of the phonon mode j (including two transverse acoustic modes and one longitudinal acoustic mode), respectively. According to the Matthiessen rule,[26] the phonon relaxation time is mainly determined by boundary scattering and the three-phonon umklapp scattering processes:

$$1/\tau = 1/\tau_b + 1/\tau_u$$

Here, τ_b and τ_u represent the relaxation time parameters for boundary scattering and the three-phonon umklapp scattering process, respectively. Similar to the SWNT,[26] the increase in the diameter of the STs is assumed to decrease the average group velocity and to augment the probability of the umklapp process, which will degrade the thermal conductivity in the STs. This observation also explains the lower κ value observed for the ST with longer constituent SWNTs (right-hand panel of Fig. 2a). The enhancement in the thermal transport properties from the smaller junction phonon scattering (originating from the longer constituent SWNTs) is much smaller than the degrading effect resulting from the increased diameter of the STs. Therefore the

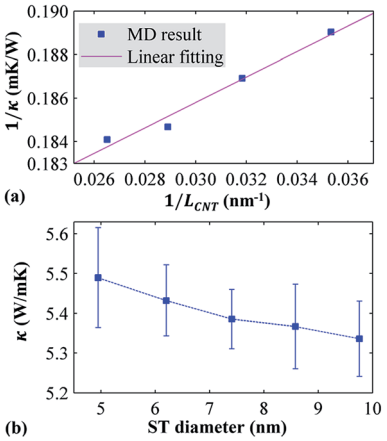

Fig. 3 Results obtained from different ST(*N*,0)@(8,0)-γ. (a) Inverse of the thermal conductivity as a function of the inverse of the length of the STs for ST(5,0)@(8,0)-γ. (b) Thermal conductivity as a function of the diameter of the ST (outer diameter).

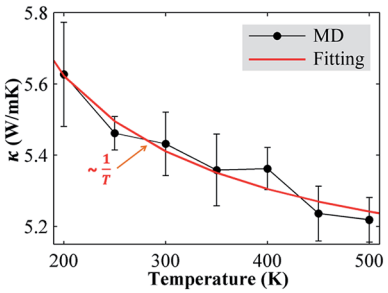

Fig. 4 Effective thermal conductivity of ST(5,0)@(8,0)-γ as a function of temperature.

STs with longer constituent SWNTs show smaller κ values. The observed dependency of the thermal conductivity on the geometrical size also explains the large difference in κ estimated between the similar "super" STs in Fig. 2a [ST(6,0)@(6,6) and ST(5,0)@(8,0)].

We also assessed the thermal conductivity of the STs at different temperatures. Fig. 4 shows that the effective κ was approximately proportional to the inverse of the temperature, which is consistent with the results reported for SWNTs.[27,28] It is expected that, as the temperature increases, the higher energy phonons will be thermally populated, which will enhance the role of umklapp scattering in determining κ (*i.e.* τ_u will dominate the overall phonon relaxation time τ). According to eqn (2), although the umklapp process dominates the phonon process in a ST, the corresponding relaxation rates increase rapidly, which will result in a continuously decreasing κ value (Fig. 4).

3.3 Influence of strain

We also examined the effect of strain on the thermal transport properties of the STs. A constant strain rate of 0.0002 ps^{-1} was adopted to elongate/compress the STs to achieve a strain from −2% (compression) to +5% (tension) after relaxation. The STs were still in the elastic deformation regime in this strain range (see ESI†). The same simulations were performed to estimate the thermal conductivity of the strained STs.

Fig. 5 shows the relative κ of ST(5,0)@(8,0)-γ and a (8,0) SWNT as a function of axial strain. The relative κ of the STs fluctuates around one, indicating insignificant effects from the axial strain on its thermal conductivity. However, for a (8,0) SWNT, the increasing strain from negative (compression) to positive (tension) values causes a significant reduction in the thermal conductivity. Such observations are consistent with the VDOS results as shown in Fig. 5b and c. For the SWNTs, the axial stain softens the high-frequency phonon modes (*i.e.* the G-band phonon modes), which decreases the specific heat and leads to a continuous reduction in κ (from compressive strain to tensile strain). However, for the STs, the low-frequency and high-frequency phonon modes are almost unchanged at different strains. This indicates that the strain has a marginal influence on the thermal conductivity. More specifically, for the ST under axial strain, its constituent SWNTs are either compressed or stretched, depending on their orientation. Taking the tensile stain as an example, the constituent SWNTs along the loading direction will be under tensile deformation, while the SWNTs along the lateral direction will be under compressive deformation as a result of the Poisson ratio (inset, Fig. 5a). In other words, the enhancement and degradation effects from the compressed and stretched SWNTs will compensate each other, resulting in the thermal conductivity of the ST being insensitive to the axial strain.

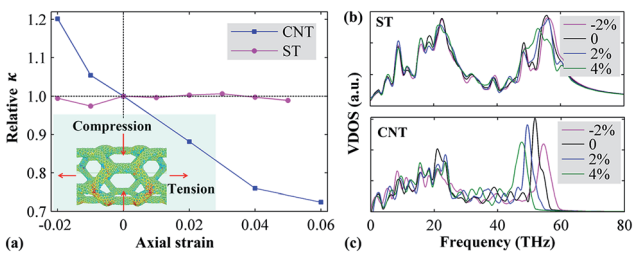

Fig. 5 (a) Relative thermal conductivity of ST(5,0)@(8,0)-γ and the SWNTs as a function of axial strain. Comparisons of VDOS at different axial strains for (b) STs and (c) SWNTs.

4. Conclusions

Based on a series of *in silico* studies, we investigated the possible tuning of the thermal conductivity of the CNT-based STs by altering the geometrical structure, size, temperature and strain. It was found that the STs with different connecting carbon rings had different VDOS spectrums, which gave different values for the thermal conductivity. Further studies showed that the STs with longer constituent SWNTs and larger diameters had a smaller thermal conductivity, which was considered to result from the decreased average group velocity and augmented probability of the umklapp process. Consistent with previous studies, the inverse of the thermal conductivity was proportional to the frequency of the scattering events – that is, the inverse of the κ value of the STs showed a good linear relationship with the inverse of the length. The effective κ shows an approximately proportional relationship with the inverse of the temperature: $\kappa \propto T^{-1}$. Additional tests showed that the thermal conductivity of the STs was insensitive to the axial strain due to its Poisson ratio – that is, due to the compensation of the enhancement and degradation effects from the simultaneously compressed and stretched SWNTs under axial strain. This study provides a fundamental understanding of the thermal transport properties of the STs and may guide their future design/fabrication and engineering applications.

Acknowledgements

Support from the ARC Discovery Project (DP130102120) and the high performance computer resources provided by the Queensland University of Technology are gratefully acknowledged. Dr Zhan is grateful to Dr Zhou from Hefei University of Technology (China) for providing advice for constructing the models.

References

1 M. A. McEvoy and N. Correll, Materials That Couple Sensing, Actuation, Computation, and Communication, *Science*, 2015, **347**, 1261689.
2 K. Ekinci and M. Roukes, Nanoelectromechanical Systems, *Rev. Sci. Instrum.*, 2005, **76**, 061101.
3 F. Bonaccorso, L. Colombo, G. Yu, M. Stoller, V. Tozzini, A. C. Ferrari, R. S. Ruoff and V. Pellegrini, Graphene, Related Two-Dimensional Crystals, and Hybrid Systems for Energy Conversion and Storage, *Science*, 2015, **347**, 1246501.
4 C. J. Shearer, A. Cherevan and D. Eder, Application and Future Challenges of Functional Nanocarbon Hybrids, *Adv. Mater.*, 2014, **26**, 2295–2318.
5 H. Zhan, Y. Zhang, J. M. Bell, Y.-W. Mai and Y. Gu, Structure-ediated Thermal Transport of Monolayer Graphene Allotropes Nanoribbons, *Carbon*, 2014, **77**, 416–423.
6 J. Niu, M. Li and Z. Xia, Growth Mechanisms and Mechanical Properties of 3d Carbon Nanotube-Graphene Junctions: Molecular Dynamic Simulations, *RSC Adv.*, 2014, **4**, 33848–33854.
7 R. Lv, E. Cruz-Silva and M. Terrones, Building Complex Hybrid Carbon Architectures by Covalent Interconnections: Graphene–Nanotube Hybrids and More, *ACS Nano*, 2014, **8**, 4061–4069.
8 R. K. Paul, M. Ghazinejad, M. Penchev, J. Lin, M. Ozkan and C. S. Ozkan, Synthesis of a Pillared Graphene Nanostructure: A Counterpart of Three-Dimensional Carbon Architectures, *Small*, 2010, **6**, 2309–2313.
9 H. F. Zhan, G. Zhang, J. M. Bell and Y. T. Gu, Thermal Conductivity of Configurable Two-Dimensional Carbon Nanotube Architecture and Strain Modulation, *Appl. Phys. Lett.*, 2014, **105**, 153105.
10 R. Zhou, R. Liu, L. Li, X. Wu and X. C. Zeng, Carbon Nanotube Superarchitectures: An Ab Initio Study, *J. Phys. Chem. C*, 2011, **115**, 18174–18185.
11 V. R. Coluci, D. S. Galvao and A. Jorio, Geometric and Electronic Structure of Carbon Nanotube Networks:'Super'-Carbon Nanotubes, *Nanotechnology*, 2006, **17**, 617.
12 Z. Qin, X.-Q. Feng, J. Zou, Y. Yin and S.-W. Yu, Superior Flexibility of Super Carbon Nanotubes: Molecular Dynamics Simulations, *Appl. Phys. Lett.*, 2007, **91**, 043108.
13 L. Ying, Q. XinMing, Y. Fan, W. Xi-Shu and Y. Yajun, Ultra-High Sensitivity of Super Carbon-Nanotube-Based Mass and Strain Sensors, *Nanotechnology*, 2008, **19**, 165502.
14 V. R. Coluci, N. M. Pugno, S. O. Dantas, D. S. Galvao and A. Jorio, Atomistic Simulations of the Mechanical Properties Of'super'carbon Nanotubes, *Nanotechnology*, 2007, **18**, 335702.
15 Y. Li, X. Qiu, F. Yang, X.-S. Wang, Y. Yin and Q. Fan, Chirality Independence in Critical Buckling Forces of Super Carbon Nanotubes, *Solid State Commun.*, 2008, **148**, 63–68.
16 M. P. Nicola, Mimicking Nacre with Super-Nanotubes for Producing Optimized Super-Composites, *Nanotechnology*, 2006, **17**, 5480.
17 F. Muller-Plathe, A Simple Nonequilibrium Molecular Dynamics Method for Calculating the Thermal Conductivity, *J. Chem. Phys.*, 1997, **106**, 6082–6085.
18 W. G. Hoover, Canonical Dynamics: Equilibrium Phase-Space Distributions, *Phys. Rev. A*, 1985, **31**, 1695–1697.
19 S. Nosé, A Unified Formulation of the Constant Temperature Molecular Dynamics Methods, *J. Chem. Phys.*, 1984, **81**, 511.
20 D. W. Brenner, O. A. Shenderova, J. A. Harrison, S. J. Stuart, B. Ni and S. B. Sinnott, A Second-Generation Reactive Empirical Bond Order (Rebo) Potential Energy Expression for Hydrocarbons, *J. Phys.: Condens. Matter*, 2002, **14**, 783.
21 S. Plimpton, Fast Parallel Algorithms for Short-Range Molecular Dynamics, *J. Comput. Phys.*, 1995, **117**, 1–19.
22 J. Dickey and A. Paskin, Computer Simulation of the Lattice Dynamics of Solids, *Phys. Rev.*, 1969, **188**, 1407.
23 A. A. Balandin, Thermal Properties of Graphene and Nanostructured Carbon Materials, *Nat. Mater.*, 2011, **10**, 569–581.
24 P. K. Schelling, S. R. Phillpot and P. Keblinski, Comparison of Atomic-Level Simulation Methods for Computing Thermal Conductivity, *Phys. Rev. B: Condens. Matter Mater. Phys.*, 2002, **65**, 144306.
25 H. F. Zhan, Y. Y. Zhang, J. M. Bell and Y. T. Gu, Thermal Conductivity of Si Nanowires with Faulted Stacking Layers, *J. Phys. D: Appl. Phys.*, 2014, **47**, 015303.
26 J. X. Cao, X. H. Yan, Y. Xiao, Y. Tang and J. W. Ding, Exact Study of Lattice Dynamics of Single-Walled Carbon Nanotubes, *Phys. Rev. B: Condens. Matter Mater. Phys.*, 2003, **67**, 045413.
27 J. X. Cao, X. H. Yan, Y. Xiao and J. W. Ding, Thermal Conductivity of Zigzag Single-Walled Carbon Nanotubes: Role of the Umklapp Process, *Phys. Rev. B: Condens. Matter Mater. Phys.*, 2004, **69**, 073407.
28 E. Pop, D. Mann, Q. Wang, K. Goodson and H. Dai, Thermal Conductance of an Individual Single-Wall Carbon Nanotube above Room Temperature, *Nano Lett.*, 2006, **6**, 96–100.

